Article

Monitoring of Dry Bands and Discharge Activities at the Surface of Textured Insulators with AC Clean Fog Test Conditions

Mohammed El Amine Slama [1,*], **Maurizio Albano** [1], **Abderrahmane Manu Haddad** [1], **Ronald T. Waters** [1], **Oliver Cwikowski** [2], **Ibrahim Iddrissu** [2], **Jon Knapper** [3] and **Oliver Scopes** [3]

1   Advanced High Voltage Engineering Centre, School of Engineering, Cardiff University, Queen's Buildings, The Parade, Cardiff CF24 3AA, UK; albanoM@cardiff.ac.uk (M.A.); haddad@cardiff.ac.uk (A.M.H.); watersrt@cardiff.ac.uk (R.T.W.)
2   National Grid plc, Warwick CV34 6DA, UK; oliver.cwikowski@nationalgrid.com (O.C.); Ibrahim.Iddrissu@nationalgrid.com (I.I.)
3   Allied Insulators Ltd., Staffordshire ST6 4HN, UK; jon.knapper@alliedinsulators.com (J.K.); oliver.scopes@alliedinsulators.com (O.S.)
*   Correspondence: slamame@cardiff.ac.uk

Abstract: The aim of this study is the presentation of the results of an in-lab comparative study of electrical and thermal monitoring of artificially polluted, HTV-textured silicone rubber insulators, with different pollution levels. This work is a preliminary study of an in-situ monitoring of 400 kV SiR textured in a polluted environment. The results showed that the rms leakage current magnitude and pulses, and the average dissipated power depended on the pollution levels and the dry-bands formation. The discharge activity and their nature are governed by the pollution level and the voltage. A differentiation and a quantification between dry-band discharge onset and dry-band arc inception is highlighted.

1. Introduction

Optimization of overhead line insulators is one of the key parameters for a high reliability of high voltage (HV) electrical grids. Flashover (FOV) of polluted transmission line insulators is one of the main problems faced by HV overhead line engineers. The performances of insulators under polluted conditions constitute the key factors in the design and dimensioning of HV insulators. The pollutant deposits covering the insulating surfaces can engender a considerable decrease of the dielectric strength of the systems, which can lead to FOVs. According to IEC 60815-1 [1], the FOV process is divided into six phases described separately below. In nature, these phases are not distinct but tend to merge. Depending on the material properties used (ceramic/glass or polymeric), the FOV process of insulators is greatly affected by the insulator's surface properties (hydrophilic or hydrophobic). In the case of glass and ceramic insulators, the surface is hydrophilic, while it is hydrophobic for polymeric insulators. The process of pollution FOV on hydrophilic surfaces begins with the deposition of a contaminant layer (containing salt, insolubles) at the insulator surface. If the pollution is nonconductive (high resistance) when dry, some wetting process is necessary before FOV occurs. In the case of coastal areas, the contaminant is already salted and wetted (salt fog). The second phase of the process is the wetting of the contamination layer according to different mechanisms (fog, light rain, condensation). The salts present in the pollution layer are dissolved and a leakage current (LC) appears and flows at the insulator surface. As the LC flows, a heating effect starts, which dries out parts of the pollution layer. This occurs where the current density is the highest, i.e., where the insulator is at its narrowest. These result in the formation of what are known as

dry bands (DBs), and the current flow interrupts. When the DBs appear, discharges are incepted at their board and are electrically in series with the resistance (impedance) of the wetted pollution layer. The kind and the intensity of the discharge depend on the resistance (impedance) of the undried pollution layer. At this instant, the LC flows again and new DBs appears, accompanied with new discharges. The temperature of the Dry Band Discharges (DbDs) becomes higher and evolve to Dry Band Partial Arcs (DBPA). This implies a raising of LC magnitudes and pulses. Depending on the balance between the gradient or the resistance (impedance) of the pollution layer and the DBPAs, the arcs bridging the DBs are sustained and might continue to propagate along the insulator surface [2]. This in turn decreases the resistance (impedance) in series with the arcs, increasing the current until it reaches a critical magnitude, and then, the insulator is completely bridged, and a line-to-earth fault (FOV) is established.

The mechanism of FOV of polymeric hydrophobic insulators initiated by water-droplets rather than dry-bands, was described by Karady and Shah [3]. The authors observed that the electric field changed the shape and elongated the droplets—they become flatter and more elongated. During this process, the coalescence of the droplets forms conductive filaments with a highly resistive layer around them. The elongated filaments shorten the inter-electrode distance and the electric field between them and other neighboring filaments becomes higher. DbDs are initiated between the filaments that lead to a local loss of hydrophobicity, which makes it easier to form new wet regions by the expansion of droplet filaments. In the end, a continuous polluted conductive layer is constituted and the DbDs extends and becomes DBPAs. Then, the situation is similar to the FOV of the hydrophilic surface.

Development of DBs formation and DbDs/DBPAs were studied in [4] for conventional non-textured insulators. They described dynamic DBs and DbDs/DBPAs by IR and visual cameras recording. According to their results, a low LC of only a few mA is enough to create the first DB. They also found that the surface temperature of the pollution layer in the DBs is only a few degrees Celsius above ambient, and is the main cause to prevent rewetting. On the other hand, they observed that DdDs are the probable cause of the delayed re-humidifying of the bands and DBPAs that might result in FOV developing from and across the DbDs.

Many studies were carried out regarding the performances and the optimization of polymeric insulators. Material characteristics as well as geometry and profiles were investigated [5,6]. However, like all polymers, they are vulnerable to long-term degradation due to aging and weathering [7–10]. Field and laboratory experiences showed that the shank regions of polluted polymeric insulators are vulnerable to partial arcs thermal damages [11]. To alleviate this problem, a textured polymeric insulator is one of the promising solution. The main advantage of this kind of insulators is the reduction of both LC density and electrical field strength in such regions, and by the same means to achieve an increase in creepage length [12–14].

In a previous work [15], DBs formation and DbDs/DBPAs at the surface of textured insulator flat samples during an AC inclined plane test was discussed. In this study, dynamic of DBs formation and DbDs/DBPAs at the surface of industrial textured insulator prototype fabricated by our partners Allied Insulators Ltd. was investigated and discussed.

2. Experimental Setup and Procedure

The fog chamber (Figure 1) is the same as described in [12–14]. The test circuit diagram is presented in Figure 2. A Hipotronics AC Dielectrics Test Set supplied the test voltage through a 150 kVA, 50 Hz transformer that could supply a 2 A load at 50 kV (1). The maximum voltage output was 75 kV. The voltage was measured with an embedded digital display on the control panel by tapping on the transformer and externally with a North Star VD-100 RC compensated division high voltage probe (2) of a standard divider ratio 10,000:1 and a <1% error specification. The leakage current was measured through a shunt

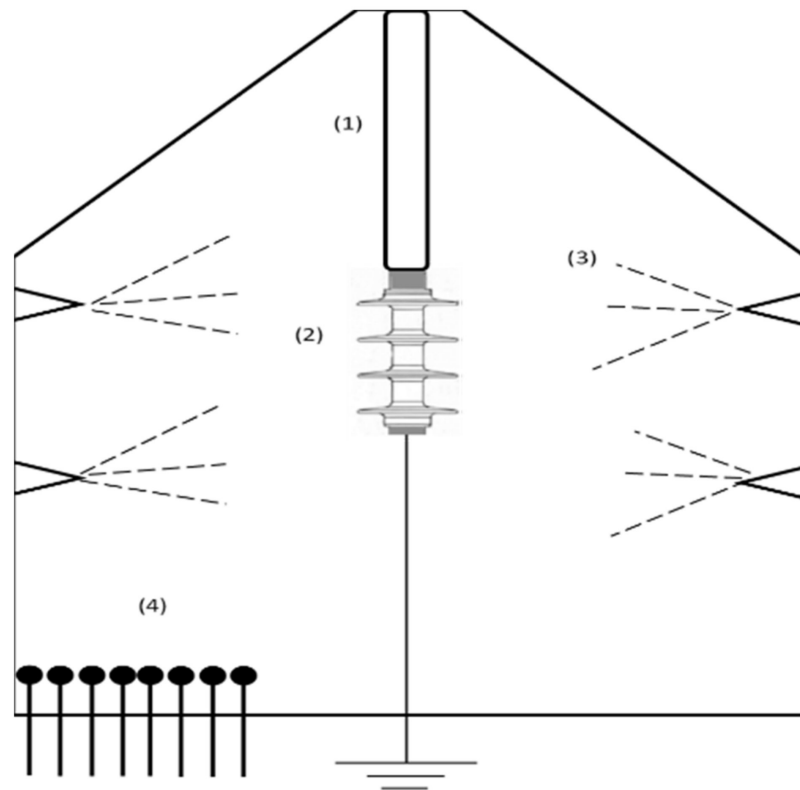resistance box (3). An optical link system was used for the connection to the data acquisition system (4).

Figure 1. Schematic view of the fog chamber. (**1**) Voltage supply conductor, (**2**) Test insulator, (**3**) Nozzles, and (**4**) Fog control panel.
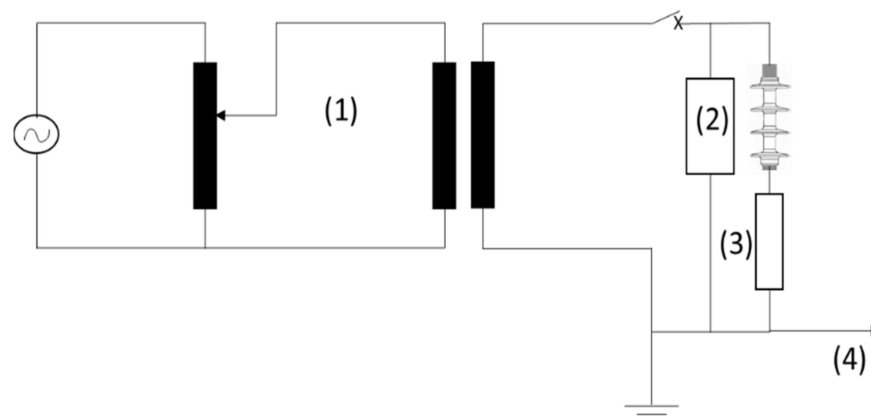

Figure 2. Diagram of the test circuit. (**1**) Voltage supply conductor, (**2**) Test insulator, (**3**) Shunt resistor, and (**4**) to DAQ system.

Applied voltage and leakage current waveforms and signals were acquired, monitored, and stored using a data acquisition (DAQ) system program, based on the NI-LabVIEW platform, as described in [12–14]. Each test facility has its own DAQ system program, as illustrated in Figure 3 and is well-described in [12–14]. As these stored samples were segments of leakage current and voltage waveforms, an appropriate post-processing software program was used to analyze and assess the data recorded during the test [12–14] and was able to calculate the following electrical characteristics.
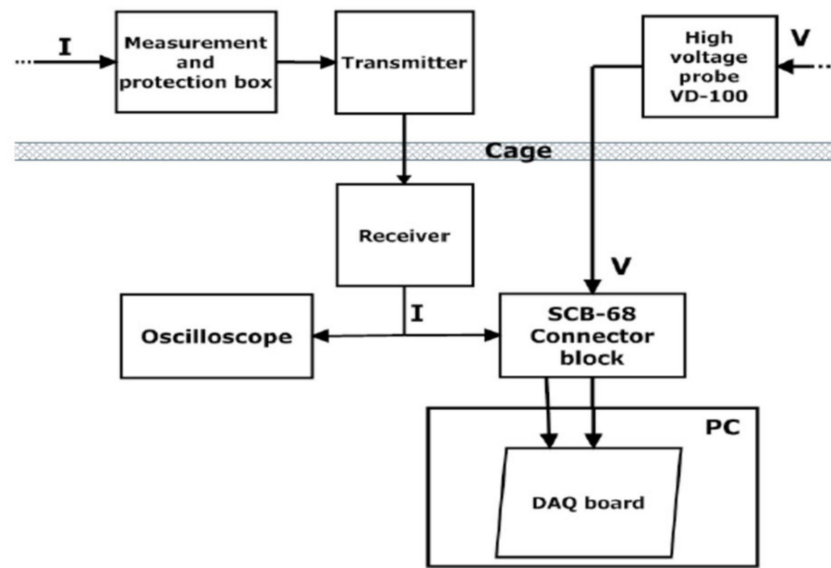
Figure 3. Data acquisition diagram. (I) current, (V) voltage and (PC) Personal Computer.

- The *r.m.s.* values of leakage current i_{rms} and voltage v_{rms} for a cycle was calculated numerically, according to Equations (1) and (2):

$$i_{rms} = \sqrt{\frac{1}{N} \cdot \sum_{j=1}^{N} i_j^2} \tag{1}$$

$$v_{rms} = \sqrt{\frac{1}{N} \cdot \sum_{j=1}^{N} v_j^2} \tag{2}$$

where i_j is the current at sample point j and N is the number of samples per cycle, which in the present work was 200.
- The surface conductance was deduced from the ratio of the current and the voltage.
- The average power was calculated for one cycle by multiplying each voltage element by its counterpart of leakage current, according to the formula:

$$p_{av} = \sqrt{\frac{1}{N} \cdot \sum_{j=1}^{N} v_j \cdot i_j} \tag{3}$$

The second recording device was an infrared (IR) camera FLIR for mapping the thermal stress on the specimen surfaces during the fog test. The standard camera calibration range was maintained, so the measurement interval was 5 °C to 150 °C for spectral thermography. An Ethernet link with a PC, established the communication with the FLIR ResearchIR Max software that processed and stored the captured IR records, and allowed control operation of the camera. A Sony camera was used to have a visual recording along the tests. During tests, heating caused by discharge activity and DB formation in the infrared spectrum were monitored. The goal of the IR imaging was to identify hot-spot formation on the insulator surface, and to correlate with electrical measurements.

The pollution constitution was sodium chloride, 40 g/L of kaolin, wetting agent (Triton), and deionized water. The conductivity of the mixture depended on the quantity of the added sodium chloride. Table 1 shows the used conductivities and their corresponding pollution level, according to IEC 60815.

Table 1. Used pollution levels.

Conductivity (mS/cm)	Pollution Level	ESDD (mg/cm^2)
1.40	Light	0.03
3.50	Medium	0.07
8.60	Heavy	0.19
12.5	Severe	0.28

Before the application of the contaminant, the insulator was pre-conditioned with brushed dry kaolin, according to the Cigré WG C4.303 [16] recommendation. This step was used for reducing the hydrophobicity of the insulator surface. Figure 4 shows an illustration of the effect of pre-conditioning on the HC index for non-textured insulators (conventional CONV). After one hour, 150 mL of contaminant was sprayed (uniform as soon as possible) along the insulator surface. Next, the insulators were left to dry vertically at ambient temperatures, during at least 24 h. The insulators were visually inspected after drying to confirm that the solid pollution layer was more-or-less uniformly formed. The geometrical parameters of the insulators are given in Table 2. Details about texture pattern and how to choose it are well-described in [11–13]. The fog air pressure and flow rate were controlled by the external fog generation control panel, as described previously. We applied a light fog rate 3 L/h (light fog) that simulated the low humidification process.
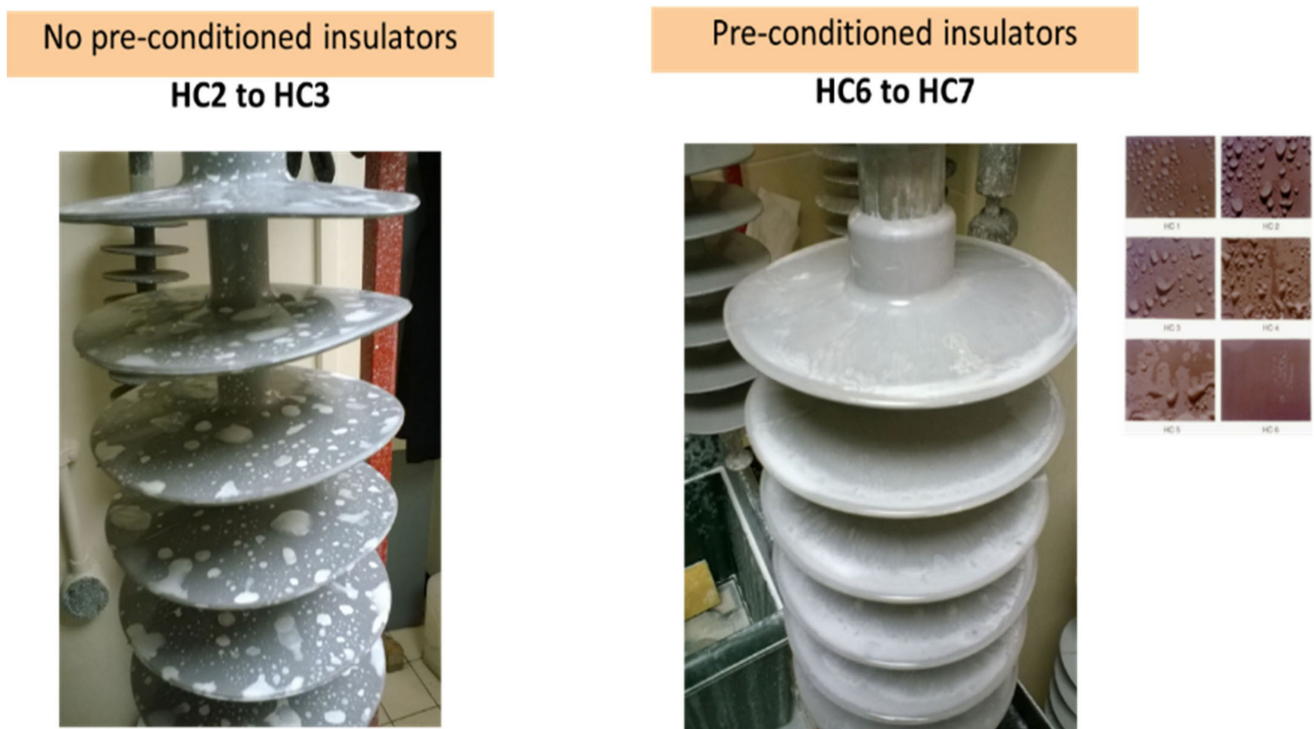
Figure 4. Examples of the effect of pre-conditioning on the HC index.

Table 2. Characteristics of the used insulators.

Arc Length (mm)	Large Shed Diameter (mm)	Small Shed Diameter (mm)	Texture Pattern (mm)	Total Surface (cm^2)
346	160	130	4	4168.6

The testing position of the polluted SiR insulator was vertical, in order to be close to the suspension insulators in the overhead lines. The fog was applied simultaneously with the test voltage. The DAQ system monitored the LC, as the pollution layer absorbed moisture and became gradually conductive. The fog input rate should be sufficient to

achieve the maximum value of layer conductance within 10–40 min of the fog application, according to the international standard IEC 60507 [17]. Low-voltage tests were performed to define the wetting duration, corresponding to the maximum SC of the pollution layer for each contamination degree. The test voltage was constant at 0.75 kV to 0.87 kV, which was the minimum voltage output of the power supply, and the retained fog rate was 3 L/h. The insulator was constantly monitored with the IR camera to detect any surface heating, in order to be sure that no drying of the pollution layer due to power dissipation, occurred during the low voltage test.

Figure 5 presents an example of used insulators for the present tests. The insulators are subdivided into 7 sheds and 8 trunk sections.
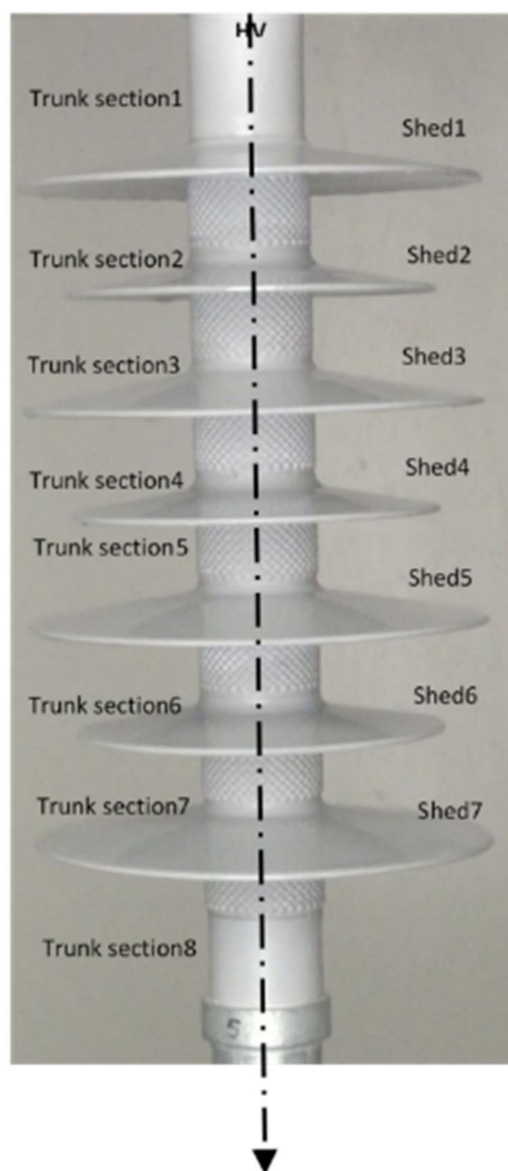

Figure 5. Photo of the used insulator.

The results of the LV tests showed that the conductance of the contaminated insulator was proportional to the pollution level, and the maximum was reached in a time interval of between 10 min and 30 min (depending on the pollution conductivity). For light pollution, the maximum conductance was reached within approximately 30 min and 25 min for medium pollution. In the case of heavy pollution, the maximum conductance was reached at 15 min, while for severe pollution the time was 10 min.

3. Results and Discussion

In this section, the voltage level and the associated SC and LC corresponding to DB onset and DbD/DBPA activity at the insulator surface were investigated.

3.1. Light Pollution

Figure 6 illustrates all steps of a voltage ramp test (from 0.87 kV to 70 kV) that were applied to a fully TXT wetted insulator and the associated LC and SC. At the first voltage steps just before 10 kV (noted (1) in Figure 6), the SC was maintained constant (2.5 µS) while the LC rose with the voltage, until approximatively 2 mA. In this step, only heating was observed without DB formation, as presented in Figure 7a. At 8 kV, the SC and the LC collapsed, resulting in a local DB formation that dramatically increased the insulator surface resistance (noted (2) in Figure 6).

According to Figure 7b, the first dry-band was localized at the beginning of the trunk Section 2 (Figure 7b). This behavior continued with voltage increase, until step (3), corresponding to the first DbD activity. The DbD activity was more intense, and other DB appeared at the other trunk sections. Those DB were larger and more active, as shown in Figure 7c,d. The maximum recorded LC at this final step was 5 mA rms. The maximum temperature at the insulator surface corresponding to DB inception was close to 22.9 °C, while it was around 32 °C when the DBs extended.
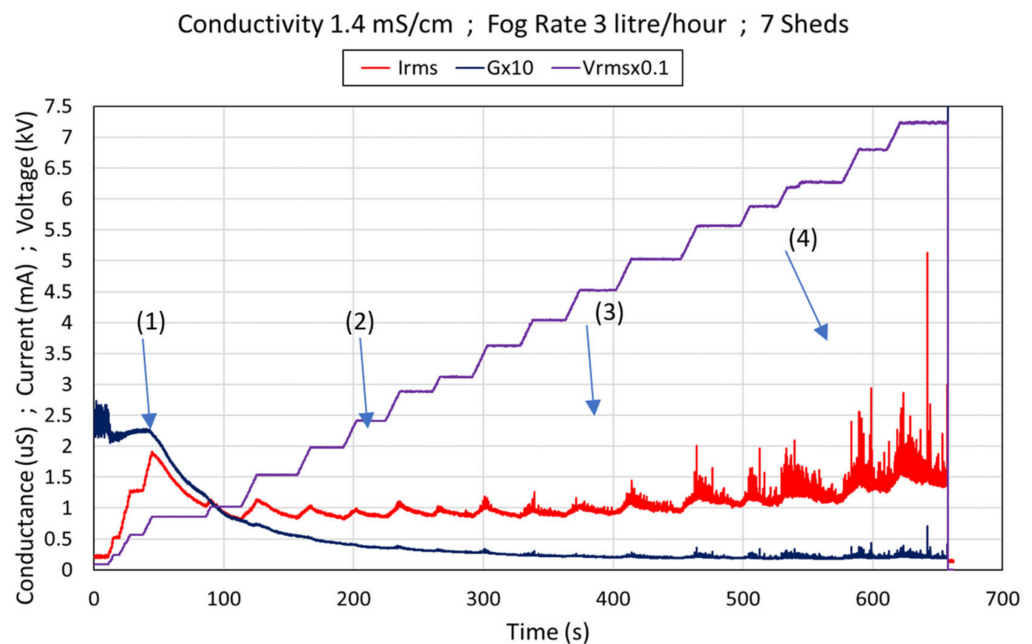

Figure 6. Surface conductance, leakage current, and applied free ramp voltage for light pollution. (1), (2) (3) and (4) are areas where LC activity and magnitude vary.

Figure 8 illustrates the DbD at the insulator surface contaminated with light pollution at the final step voltage (70 kV rms). DbDs were corona/streamers and spark, discharged with ramifications at their heads and purple/white color. Those discharges appeared at the junction between the trunk and the shed. Some discharges also appeared between the sheds due to the formation of the suspended droplets that could be assimilated as a conical electrode. The immediate consequence was that the air broke down between the droplet and the shed.

3.2. Medium Pollution Level

Figure 9 illustrates the records of LC and SC for all steps of a voltage ramp test, as shown for the light pollution level. At the first voltage steps just before 10 kV (noted (1) in Figure 9), the SC was maintained constant, while the LC increased with voltage, until

approximatively 7 mA. At 8 kV, the SC and the LC collapsed, resulting in a local DB formation that dramatically increased the insulator surface resistance. Figure 10a,b illustrates the visual and the thermal records of the formation of the first DBs and their extension at the junction of the trunk and at the top of the fourth shed.

At 18 kV, the first DbDs appeared, corresponding to the first current pulses (noted (2) in Figure 9). With an increase in applied voltage, the LC activity was more intense (noted (3) in Figure 9), with a maximum value of 12 mA rms at 27 kV rms. The DbDs were spark discharged with purple/white coloration, as presented in Figure 11a,b. Above 30 kV, the DB activity was more intense, and the LC increased with the voltage. According to Figure 9, the LC in area (4) and (5) had typical values of dry-band arcs (DBPA) and a maximum LC growth up to 40 mA rms.
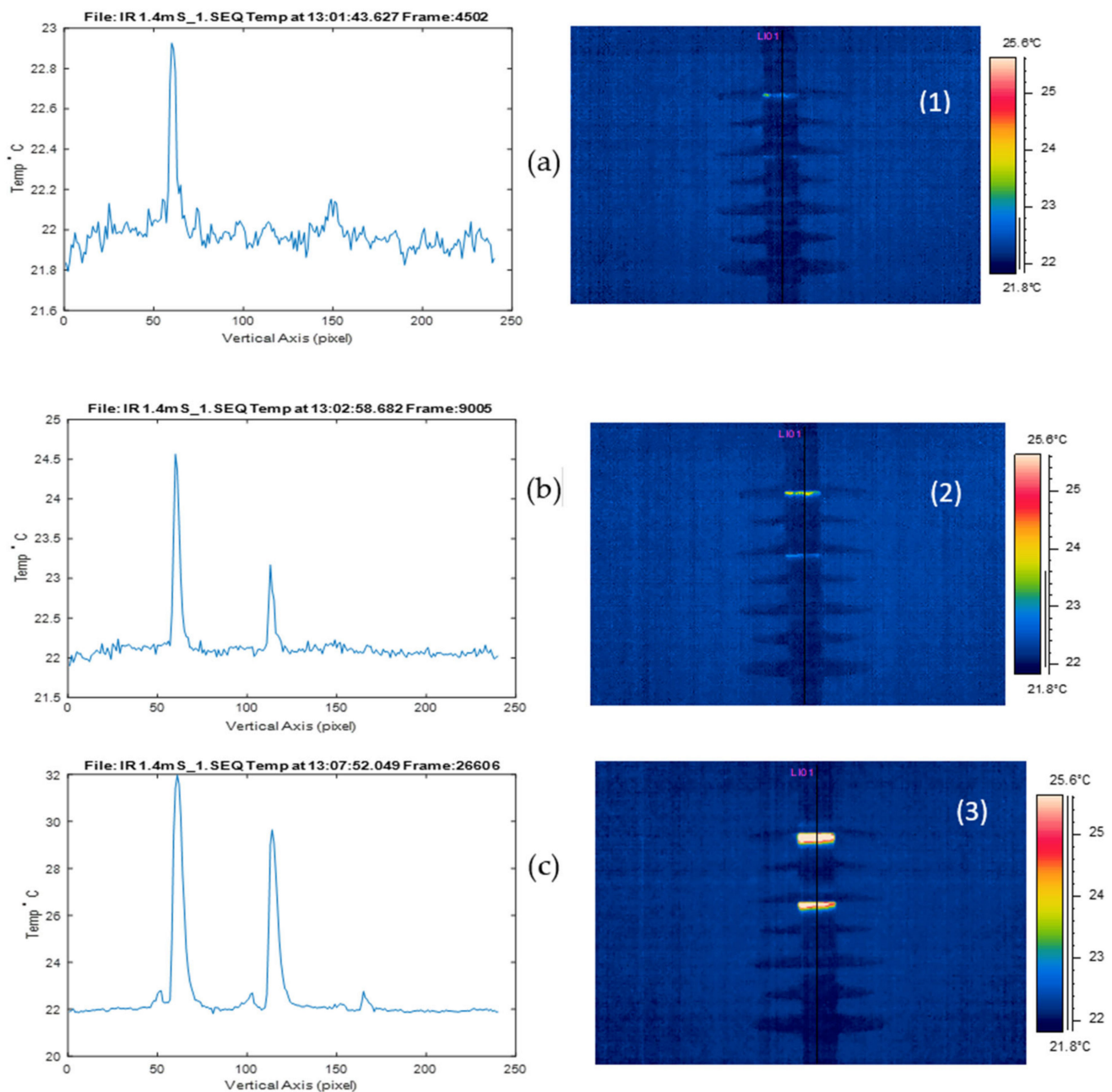

Figure 7. Thermal picture and temperature profile variation for light pollution. (**a**–**c**) are measured temperatures at the insulator surface. (1), (2) and (3) are the corresponding IR images.
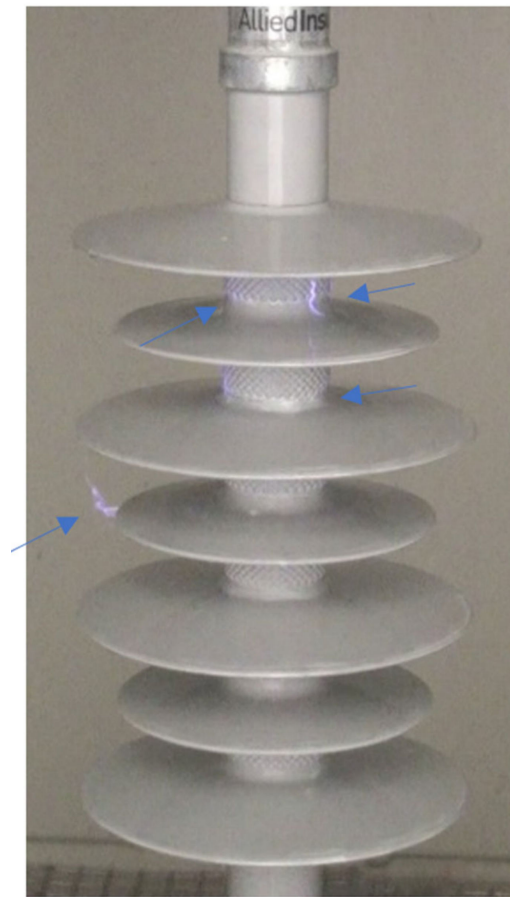
Figure 8. Visual image of Dry Band Discharges (DbD) on the insulator surface with light pollution at 70 kV rms.
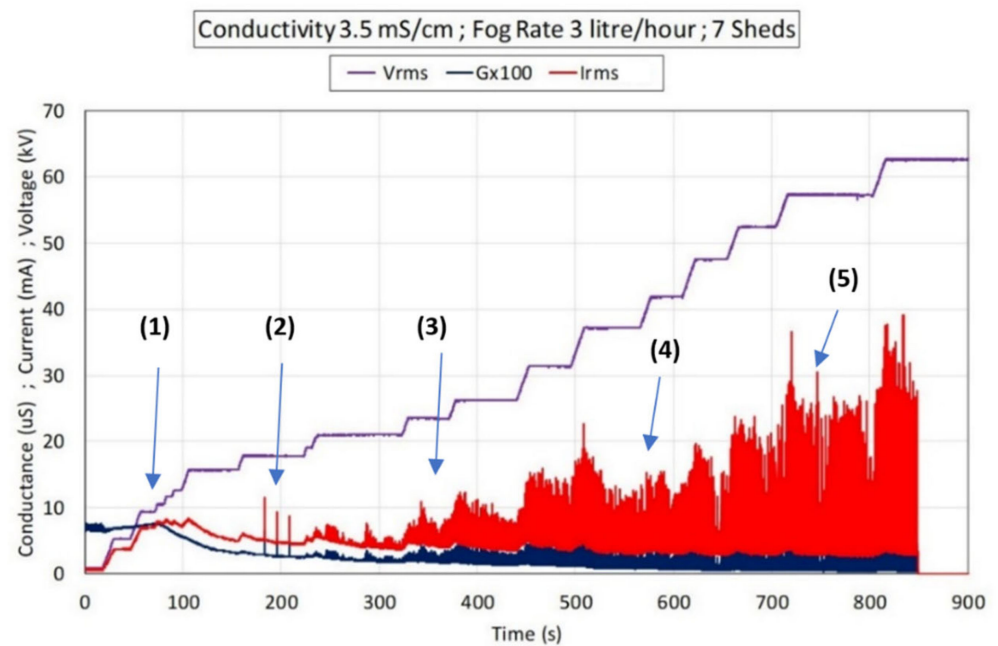

Figure 9. Surface conductance, leakage current, and applied free ramp voltage for medium pollution. (1), (2) (3), (4) and (5) are areas where LC activity and magnitude vary.
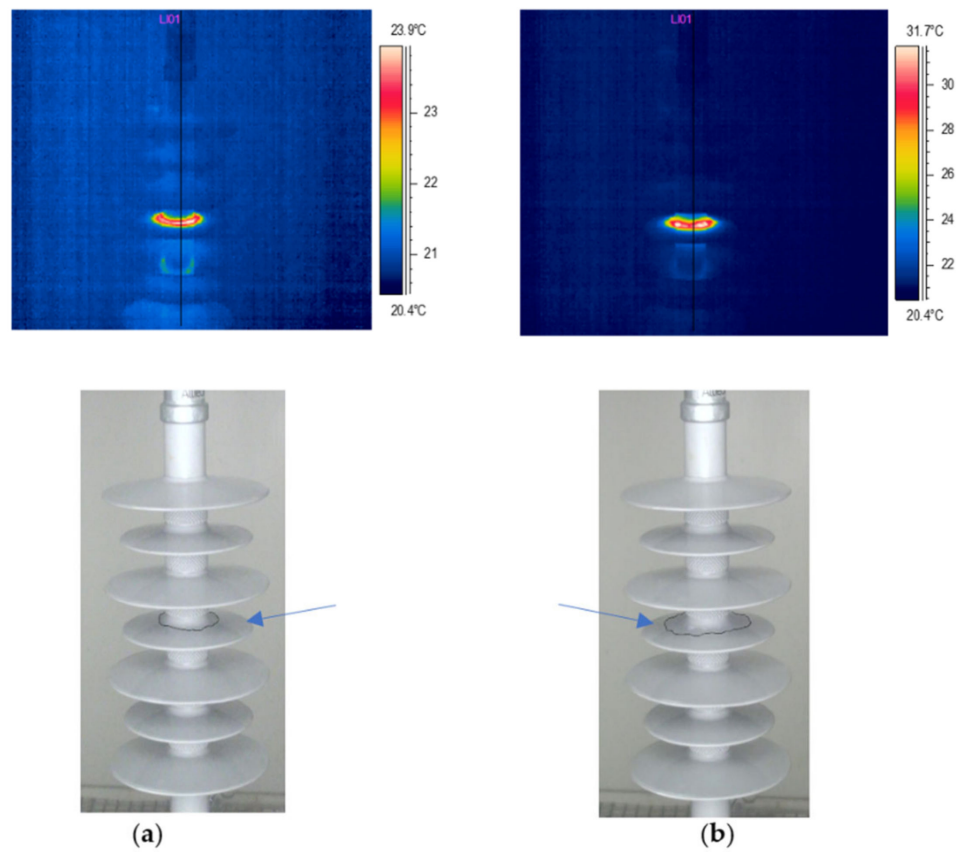
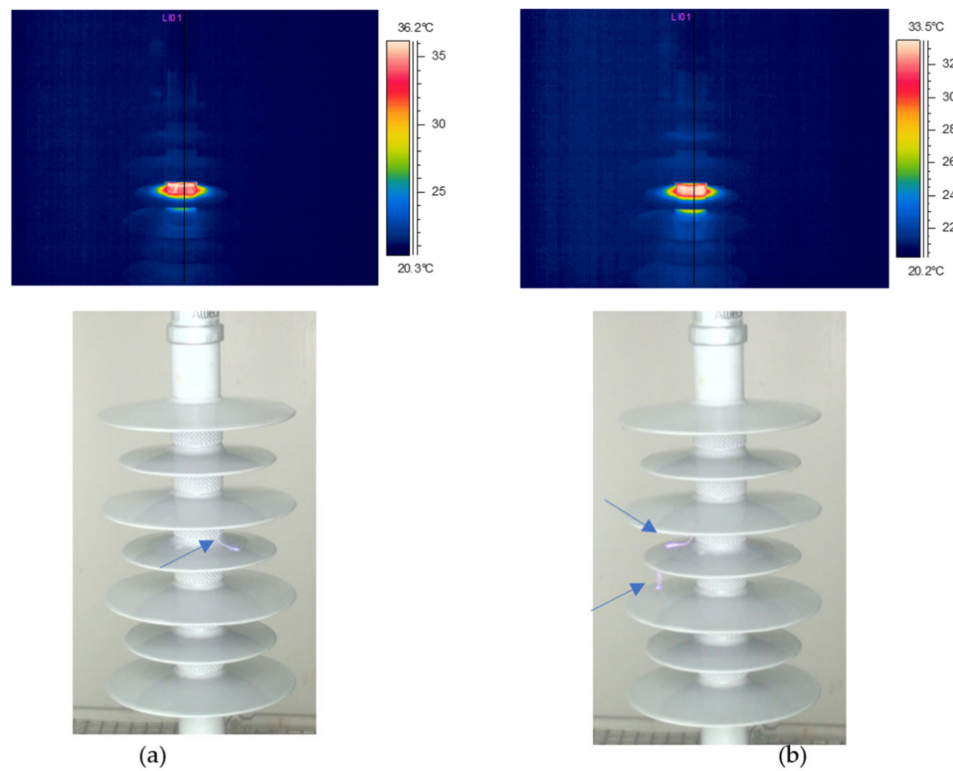**Figure 10.** Dry-band formation and extension for medium pollution. (**a,b**) represent DB extension.

Figure 11. Dry Band Discharges (DbD) development for medium pollution. (**a,b**) represent DbDs activity and their corresponding IR images.

3.3. Heavy Pollution Level

Figure 12 illustrates the recording of LC and SC for all steps of a voltage ramp test, as before. DB onset began at 5 kV rms (noted (1) in Figure 12). The SC and LC were likely constant (respectively, 0.9 μS and 5 mA). Figure 13a shows the localization and the temperature profile of the first DB onset corresponding to the area (1) of Figure 12. We remark that DB inception were localized at trunk sections 1, 4, 5, and 6. At 7 kV rms, the SC and the LC collapsed, resulting in a local DB extension, which drastically increased the insulator surface resistance. Figure 12 illustrates visual and thermal images of the DBs and their extension at the trunks of the insulator, especially trunk Section 6.
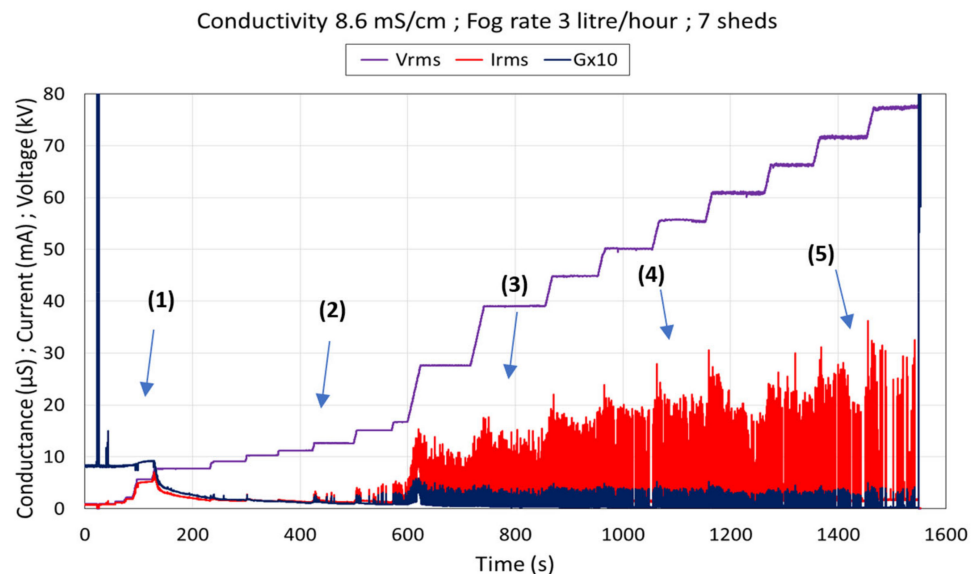

Figure 12. Surface conductance, leakage current, and applied free ramp voltage for heavy pollution. (1), (2) (3), (4) and (5) are areas where Leakage Current (LC) activity and magnitude vary.

At 12 kV, the first DbD appeared corresponding to the first current pulses (noted (2) in Figure 10). With an increase in the applied voltage, the LC activity was more intense (noted (3) in Figure 10). The LC increased drastically at 17 kV rms with a maximum of 20 mA rms. Figures 13 and 14 illustrate the thermal profile and the localization of the DbD activities and DB extension at the trunk sections of the insulator. We remark that the DB of trunk section number 6 extended and the temperature rose.

The LC increased with the applied voltage at each ramp step (noted (4) in Figure 12), with a maximum value of 36 mA rms. Figure 13 illustrates the temperature profile of the insulator, corresponding to area 4 of Figure 12. We remarked that the temperature of the trunk Section 6 was about 40 °C. Over 30 kV, the DB activity was more intense, and the LC increased with the voltage. According to Figure 12, the LC of area (5) had typical values of dry-band arcs (DBPA) and a maximum LC growth up to 40 mA rms. Figure 14 shows the DBPA activity at the insulator surface and infrared camera records of the DB and DBPA evolution. According to Figure 14, we remarked that the DBPA activity increased and many DBPAs were localized at the trunk section and between sheds. In Figure 15, the DBs extended along the trunk section and between the sheds, with voltage rising.

3.4. Severe Pollution Level

Figure 16 presents the recording of LC and SC for all steps of the voltage ramp test. The DB onset begins less than 4 kV rms (noted (1) in Figure 16). Figure 17 shows the DB onset before any discharge activity. We remarked that the DBs were initiated at trunk Sections 2, 3, and 4. The SC and LC decreased until constant values (respectively, 1.13 μS and 1.5 mA). At 16 kV, the first DBPA appeared as indicated in Figure 16 region (2). The LC activity and intensity increased with the voltage ramp steps (region (3) in Figure 16).

This increase was a consequence of the formation/extension of DB (Figure 18) and the inception and development of DBPAs (Figure 19). The LC amplitude increased with the voltage ramp steps (regions (4) and (5) of Figure 16), which indicated a high DBPA activity at the insulator surface, as presented in Figure 19. The maximum LC was around 60 mA rms at 70 kV rms.
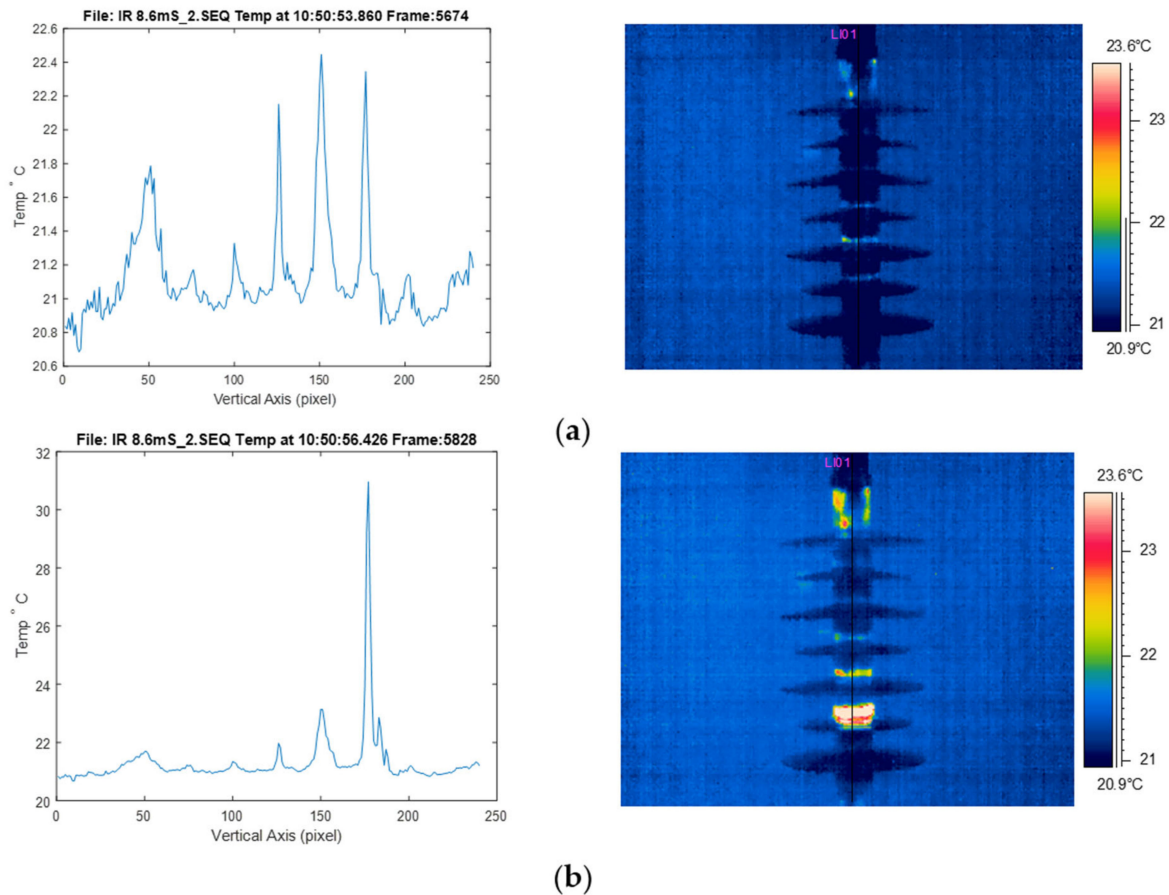

Figure 13. Dry-band onset and extension for heavy pollution (**a**,**b**) represent the (Dry-band Arcs) DBAs activity and corresponding temperature.
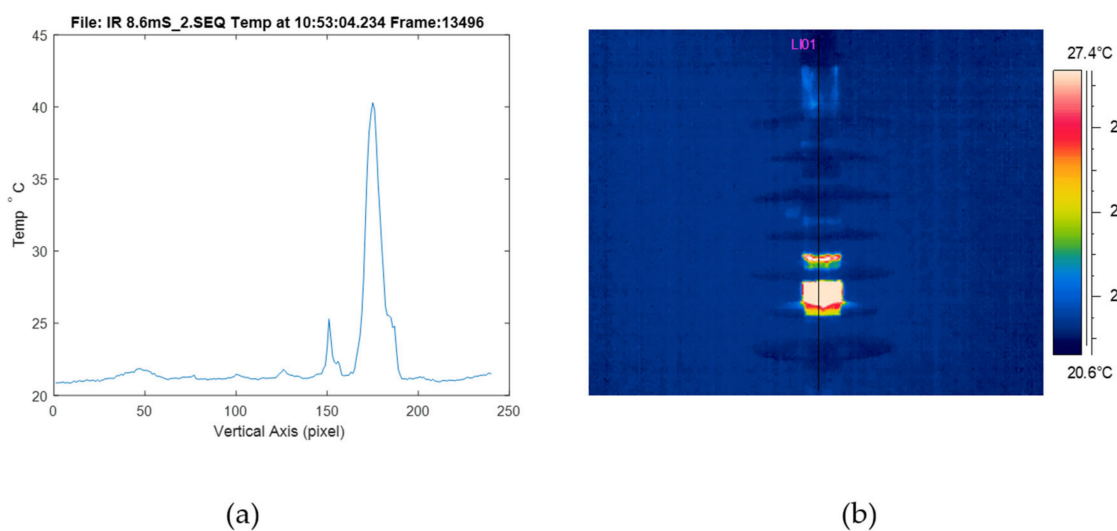

Figure 14. Temperature profile and DB evolution for heavy pollution at 30 kV rms (**a**) temperature profile (**b**) IR image.
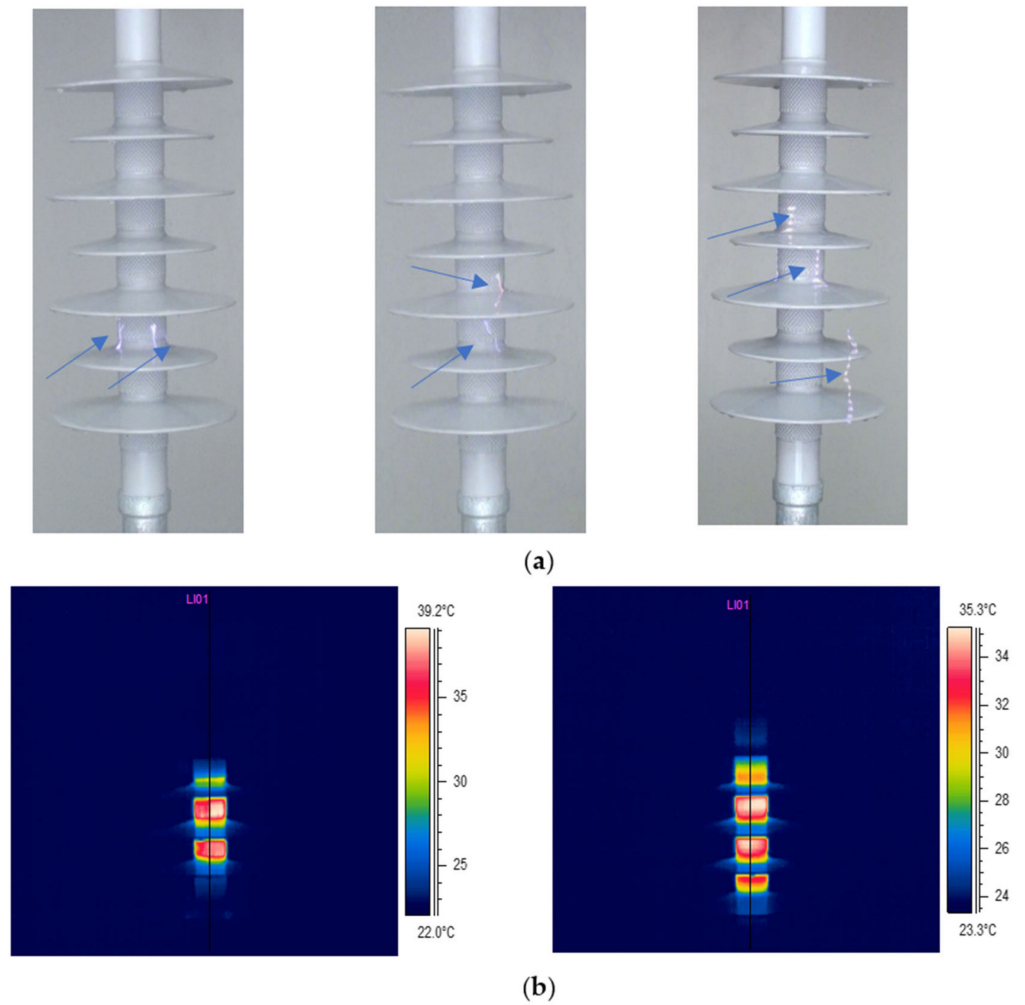
Figure 15. DBPA activity and IR images for heavy pollution over 40 kV rms (**a**) visual image of DBAs activity and (**b**) IR image of DB extension.
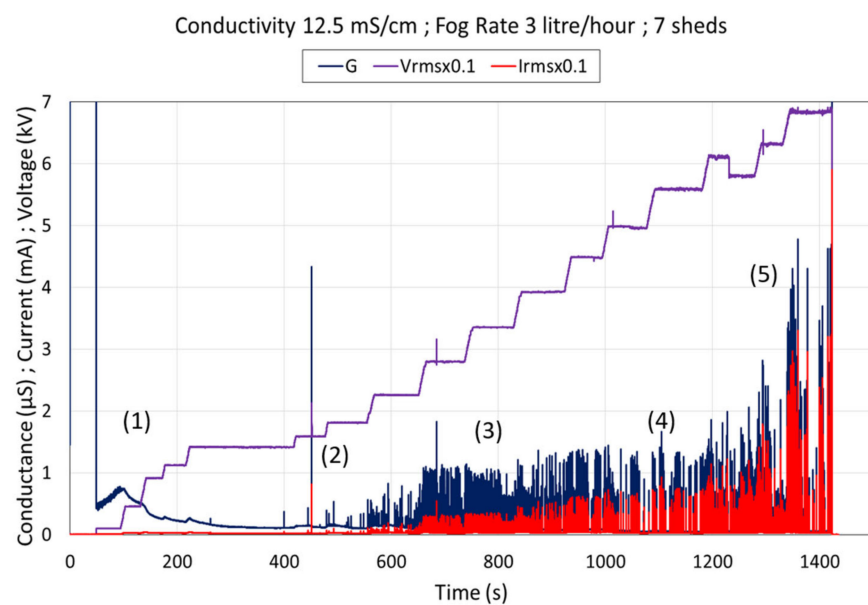

Figure 16. Surface conductance, leakage current, and applied free ramp voltage for severe pollution. Both voltage and current were divided by 10. (1), (2) (3), (4) and (5) are areas where LC activity and magnitude vary.
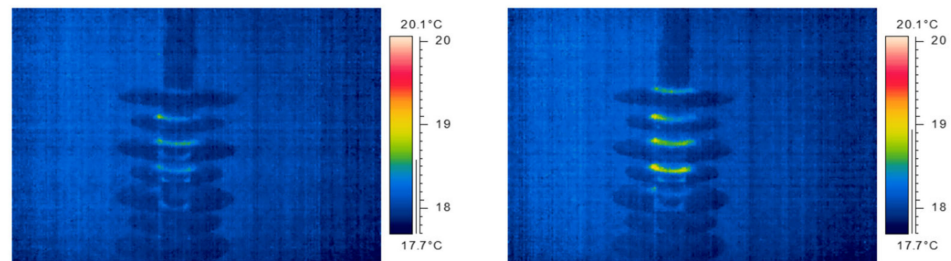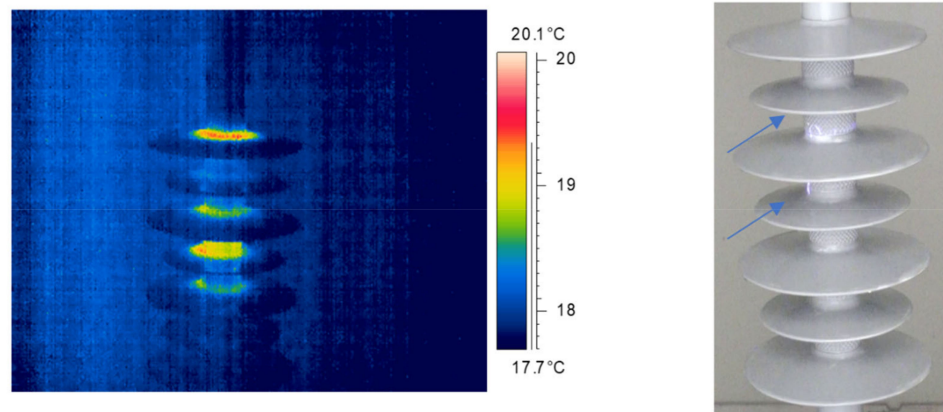
Figure 17. Dry-bands onset for heavy pollution.

Figure 18. Dry-bands and firsts discharges inception/development for heavy pollution.
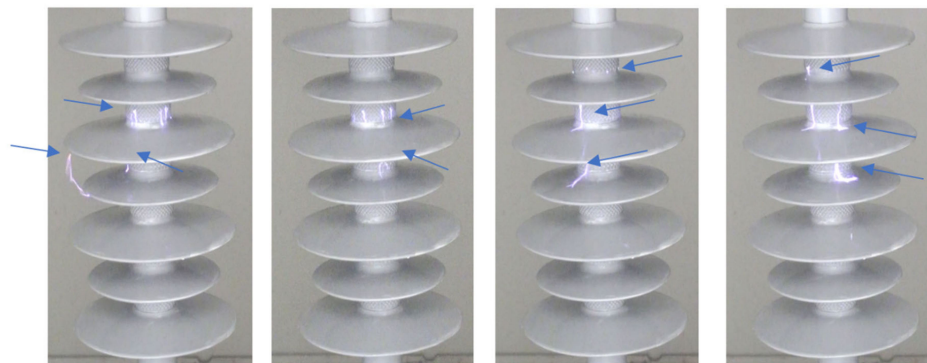

Figure 19. Discharges development with the voltage step increase for heavy pollution.

According to Figure 18, we remarked that the discharges jumped from the trunk section to the shed because of the extension of DB at the junction between these two elements.

3.5. Dry Band Voltage Onset, Dry Band Discharge Voltage Inception, and Average Power

3.5.1. DB Voltage Onset and DbD Voltage Inception

Based on previous measurements, the DB voltage onset and the DbD voltage inception were estimated and plotted as a function of ESDD. Figure 20 shows that both DB voltage onset and the DbD voltage inception decreased with the pollution level. This was attributed to the thermal dissipation of moisture from the pollution layer, which depended on its conductivity. When the conductivity increased, the current on the polluted surface was higher, and consequently, the Joule's dissipation was higher. On the other hand, the DB voltage onset appeared to be linear with the pollution level. This was due to the ohmic behavior of the equivalent electrical circuit, which behaved as a linear resistor with joules effect and heating. The DbD voltage inception presented a different trend and was more likely to be a non-linear function. The main reasons were that the discharges inception depended on many factors, such as ionization process, DBs size, rewetting, and the evaporation process [18] and the non-linearity of the discharge resistance [19].
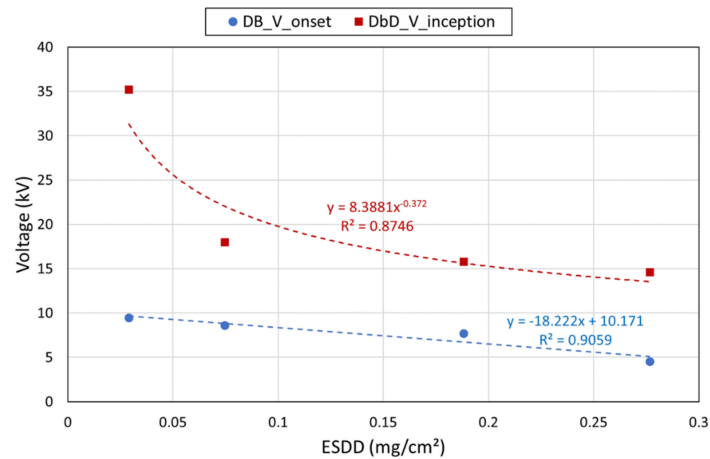
Figure 20. Dry Band (DB) voltage onset and Dry Band Partial Arcs (DBPA) voltage inception vs. pollution level.

3.5.2. Average Power

According to Figure 21a–d, the average power (AP) increased with the pollution layer conductivity. For example, in the case of light pollution, the AP corresponding to DB onset was approximately 16 W, whilst at the DbD inception, it was around 34 W. The maximum AP was 240 W at 70 kV rms. In the case of severe pollution, the AP corresponding to DB onset was approximately 4.5 W, while it was approximately 20 W at the DbD inception. The maximum AP was close to 1 kW for 70 kV rms. According to these results, the energy dissipated for the formation of DBs was less than that needed for the DbDs inception. However, the dissipated energy increased with the voltage and the pollution level.
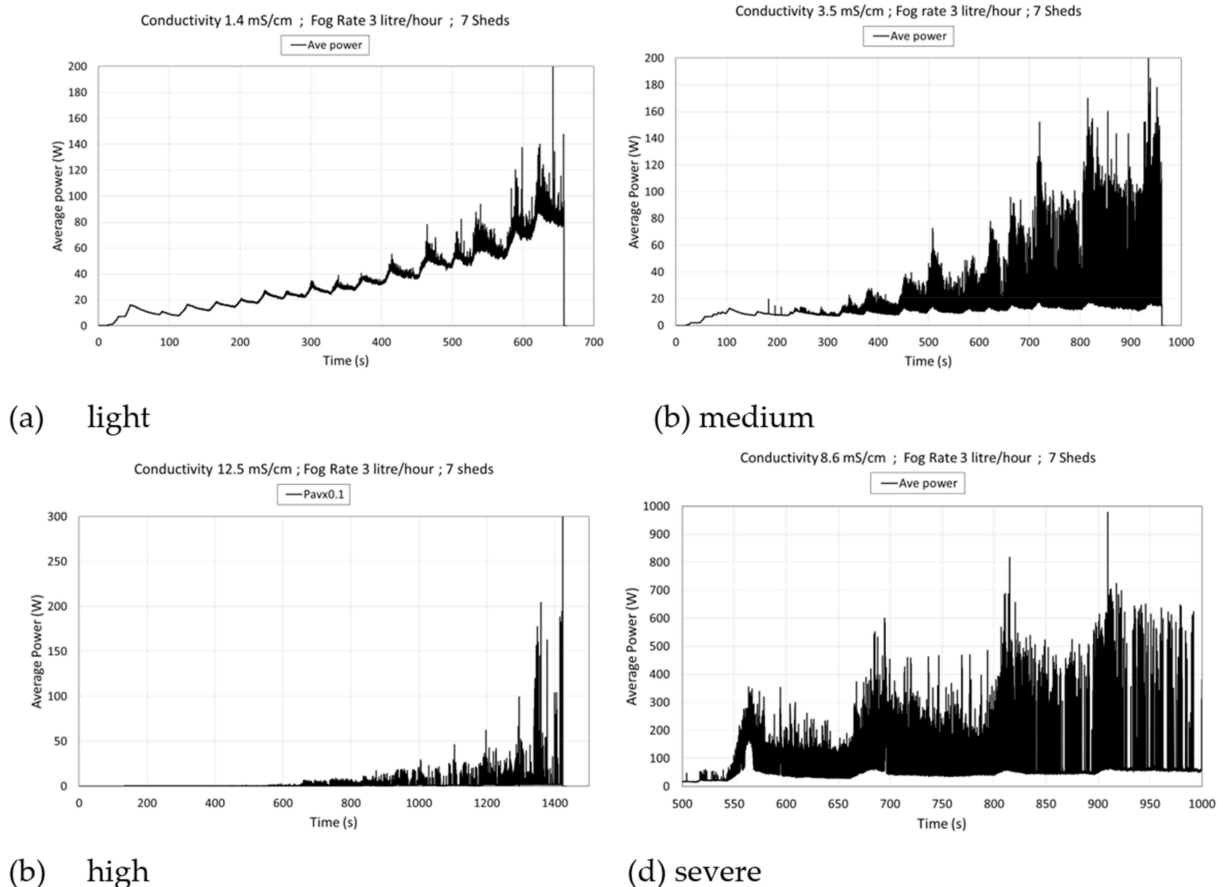

(a) light

(b) medium

(b) high

(d) severe

Figure 21. Calculated average power for various pollution levels. (**a**–**d**) are the pollution levels.

4. Conclusions

This study described the dynamic of LC, DB, DbDs, and DBAs of SiR textured insulators under clean fog test conditions. The results showed that the LC rms magnitude and the average power dissipation depended on the pollution level. Additionally, the following results were deduced:

- DB onset began at a relative low voltage (less than 10 kV), depending on the pollution layer conductivity. At this stage, the SC and LC were likely constant.
- After this stage, with increasing voltage ramp step, the SC and LC collapsed, resulting in local DB extension, which drastically increased the insulator surface resistance. Visual and thermal images showed that the DBs were situated at the trunks of the insulator.
- The DbD appeared at a voltage greater than the DB onset. With the increase of the applied voltage, the LC activity was more intense.
- The DbD were spark discharged with purple/white coloration and partial arcs with orange color. The nature of the discharges depended on the voltage level and the pollution layer conductivity.
- The discharge activity was related to the temperature distribution at the insulator surface and the DB dynamic. The nature of those discharges' changed with the pollution level and the applied voltage magnitude.
- DBA inception voltage was higher than DB onset voltage and depended on the applied voltage and the temperature distribution, as well as the pollution level.

Author Contributions: Conceptualization, M.E.A.S.; methodology, M.E.A.S.; validation, M.E.A.S., A.M.H., M.A., and R.T.W.; formal analysis, M.E.A.S., A.M.H., M.A., and R.T.W.; investigation, M.E.A.S.; resources, A.M.H., M.A., O.C., O.S. and J.K.; data curation, M.E.A.S.; writing—original draft preparation, M.E.A.S.; writing—review and editing, M.E.A.S. and A.M.H.; supervision, M.E.A.S., A.M.H., M.A., and R.T.W.; project administration, A.M.H., O.C., and I.I.; funding acquisition, A.M.H. All authors have read and agreed to the published version of the manuscript.

Institutional Review Board Statement: Not applicable.

Informed Consent Statement: Not applicable.

Data Availability Statement: Not applicable.

Conflicts of Interest: The authors declare no conflict of interest.

Abbreviations

ADE	Accumulated Dissipated Energy
AP	Average Power
DB	Dry-Band
DBA	Dry-band Arc
DBPA	Dry Band Partial Arc
ESDD	Equivalent Salt Deposit Density
FOV	Flashover
HC	Hydrophobicity Class
LC	Leakage Current
SC	Surface Conductance
TXT	Textured

References

1. International Electrotechnical Commission. *Selection and Dimensioning of High-Voltage Insulators Intended for Use in Polluted Conditions—Part 1: Definitions, Information and General Principles*; IEC Technical Specification IEC/TS 60815-1, Edition 1.0, 2008-10-29; IEC: London, UK, 2008.
2. Slama, M.E.A.; Beroual, A. Flashover discharges dynamic with continuous and discontinuous pollution layer under lightning impulse stress. *Electr. Eng.* **2021**. [CrossRef]

3. Karady, G.; Shah, M.; Brown, R. Flashover mechanism of silicone rubber insulators used for outdoor insulation-I. *IEEE Trans. Power Deliv.* **1995**, *10*, 1965–1971. [CrossRef]
4. Albano, M.; Waters, R.; Charalampidis, P.; Griffiths, H.; Haddad, A. Infrared analysis of dry-band flashover of silicone rubber insulators. *IEEE Trans. Dielectr. Electr. Insul.* **2016**, *23*, 304–310. [CrossRef]
5. An, Z.; Shen, R.; Gao, W.; Gu, X.; Chen, W.; Yang, L.; Yang, W.; Zhang, Z. Improved flashover performance and tracking resistance of silicone rubber by direct fluorination. *J. Appl. Polym. Sci.* **2020**. [CrossRef]
6. Arshad, G.; Momen, M.; Farzaneh, A.; Nekahi, A. Properties and Applications of Superhydrophobic Coatings in High Voltage Outdoor Insulation: A Review. *IEEE Trans. Dielectr. Electr. Insul.* **2017**, *24*, 3630–3646. [CrossRef]
7. Gubanski, S. Modern outdoor insulation—concerns and challenges. *IEEE Electr. Insul. Mag.* **2005**, *21*, 5–11. [CrossRef]
8. Slama, M.E.A.; Beroual, A. Behaviour of AC high voltage polyamide insulators: Evolution of leakage current in different surface conditions. *Power Eng. Electr. Eng.* **2015**, *13*, 74–80.
9. Elombo, A.I.; Holtzhausen, J.P.; Vermeulen, H.; Pieterse, P.J.; Vosloo, W.L. Comparative evaluation of the leakage current and aging performance of HTV SR insulators of different creepage lengths when energized by AC, DC+ or DC– in a severe marine environment. *IEEE Trans. Dielectr. Electr. Insul.* **2013**, *20*, 421–428. [CrossRef]
10. Abed, M.E.A.; Hadi, H.; Belarbi, A.W.; Slama, M.E.A. Experimental Characterization of Electric Power Insulator Subjected to an Accelerated Environmental Ageing. *Elektrotehniski Vestn.* **2020**, *87*, 183–192.
11. Haddad, A.; Waters, R.T. Insulating Structures. U.S Patent 764268, 2011.
12. Haddad, A.; Waters, R.; Griffiths, H.; Chrzan, K.; Harid, N.; Sarkar, P.; Charalampidis, P. A new approach to anti-fog design for polymeric insulators. *IEEE Trans. Dielectr. Electr. Insul.* **2010**, *17*, 343–350. [CrossRef]
13. Waters, R.T.; Haddad, A.H.; Griffiths, H.; Harid, N.; Charalampidis, P.; Sarkar, P.K. Dry-band discharges on polluted silicone rubber insulation: Control and characterization. *IEEE Trans. Dielectr. Electr. Insul.* **2011**, *18*, 1995–2003. [CrossRef]
14. Charalampidis, P.; Albano, M.; Griffiths, H.; Haddad, A.; Waters, R. Silicone rubber insulators for polluted environments part 1: Enhanced artificial pollution tests. *IEEE Trans. Dielectr. Electr. Insul.* **2014**, *21*, 740–748. [CrossRef]
15. Slama, M.E.A.; Albano, M.; Haddad, A.; Waters, R.T. Dry-Band Discharges Dynamic at the Surface of SiR Textured Insulator During AC Inclined Plane Test. In *Proceedings of the 21st International Symposium on High Voltage Engineering*; Springer: Berlin/Heidelberg, Germany, 2019; Volume 2, pp. 504–517.
16. Working Group C4.303. *Artificial Pollution Test for Polymer Insulators. Results of Round Robin Test*; Cigré: Paris, France, 2013.
17. IEC 60507:1991. *Artificial Pollution Tests on High-Voltage Insulators to Be Used on A.C. Systems*; International Electrotechnical Commission: Geneva, Switzerland, 2014.
18. Albano, M.; Waters, R.T.; Haddad, A.; Griffiths, H. Electric field distortion at outdoor insulation in severe Environments. In Proceedings of the 19th International Symposium on High Voltage Engineering, Pilsen, Czech Republic, 23–28 August 2015.
19. Slama, M.E.-A.; Beroual, A.; Hadi, H. Analytical computation of discharge characteristic constants and critical parameters of flashover of polluted insulators. *IEEE Trans. Dielectr. Electr. Insul.* **2010**, *17*, 1764–1771. [CrossRef]